HHS Public Access

Author manuscript

Chem Commun (Camb). Author manuscript; available in PMC 2021 June 25.

Published in final edited form as:

Chem Commun (Camb). 2020 June 25; 56(51): 6977–6980. doi:10.1039/d0cc02612c.

Cell organelle targeting of near-infrared croconaine dye controls photothermal outcome†

Ying Wen[a,b], **Hannah H. McGarraugh**[a], **Cynthia L. Schreiber**[a], **Bradley D. Smith**[a,*]

[a.] Department of Chemistry and Biochemistry, 251 Nieuwland Science Hall, University of Notre Dame, Notre Dame, IN 46556, USA

[b.] Institute of Molecular Science, Shanxi University, Taiyuan 030006, China

Abstract

Near-infrared croconaine-peptide conjugates that target the cell nucleus promote photothermal induced cell death. In contrast, a croconaine-morpholine conjugate that targets the cell lysosomes promotes lysosome permeabilization without measurable cell phototoxicity.

Graphical Abstract

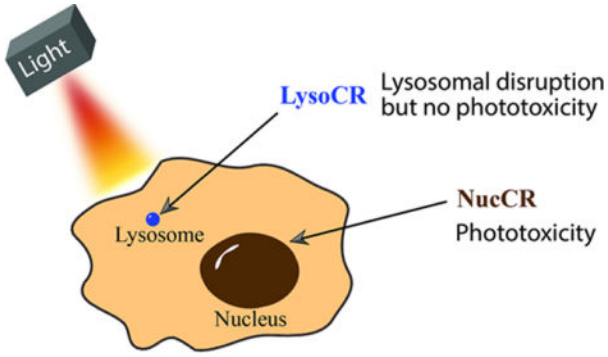

Photothermal heating the cell nucleus promotes cell death; whereas, photothermal heating the cell lysosome produces lysosomal disruption with no phototoxicity.

A typical approach to laser-induced photothermal heating is treatment of a biological sample with a photothermal agent that can selectively absorb long wavelength laser light and convert the light energy into localized heating.[1] In principle, the confined heating enables precise modulation of biological function with high spatiotemporal control.[2] A common experimental goal is to kill pathogenic cells such as cancer cells, and this technique is called Photothermal Therapy (PTT).[3,4] It is intuitive to think that the efficiency of cell killing by a photothermal agent will depend on its precise intracellular location and the proximity to

†Electronic Supplementary Information (ESI) available: Experimental section, synthesis, supplementary figures and references. See DOI: 10.1039/x0xx00000x

* smith.115@nd.edu.

Conflicts of interest

There are no conflicts to declare.

intracellular organelles.[5,6] Since the structure and physiological function of organelles varies widely, it is also likely that they will have different sensitivities to laser-induced hyperthermia, and that the outcome might vary between organelles. At present, there are very few reports of unambiguous studies that assess the sensitivities of different organelles to photothermal heating. There are two major reasons for this situation. One reason is the inability to target photothermal agents to a specific organelle. Many laser-absorbing chromophores are nanomaterials that have excellent photothermal conversion efficiencies,[3] but it is inherently challenging to convert them into targeted conjugates that can permeate cells and accumulate selectively at a specific organelle. In comparison, it is synthetically easier to convert a small molecular organic dye into an organelle targeted conjugate.[7,8] But dyes often have poor photostability and modest photothermal conversion efficiency (Table S1).[4] Furthermore, dye photoexcitation often induces a mixed photothermal and photodynamic response that leads to photogeneration of reactive oxygen species as well as local heating.[9,10] This mixed response makes it difficult to unambiguously attribute any observed laser induced effect to a specific photothermal mechanism. In 2013, we reported a potential solution to all these dye excitation problems by showing that croconaine dyes are unusually effective as near-infrared chromophores for photothermal heating.[11] An example of a simple, nontargeted croconaine dye is **PB09** (Scheme 1a) which only produces localized heating without any oxygen photosensitization or dye photobleaching.[12] This is because the croconaine excited state is extremely short-lived and undergoes rapid non-radiative decay with negligible fluorescence or intersystem crossing (and thus no oxygen photosensitization). The utility of croconaine dyes for efficient PTT of cancer has been demonstrated by several independent groups.[13–15] Here, we utilize the “clean heating” property of croconaine dyes to study the outcome of organelle targeted photothermal heating without any interfering photodynamic effect.

Inspection of the literature reveals that the majority of organelle photothermal heating studies have focused on the mitochondria as the organelle target, and this body of work has shown clearly that photothermal disruption of the mitochondria leads efficiently to cell death.[16–18] In comparison, there are far fewer studies of targeted photothermal heating of other organelles, and thus we chose to develop croconaine probes that target two less-explored organelles; namely, the nucleus and the lysosome.

The nucleus targeted croconaine probes are **NucCR** and **NucCR’** (Scheme 1b), two closely related conjugates (one linear and the other branched) that are comprised of three structural components; a croconaine photothermal chromophore, a nuclear localization signal peptide (NLS peptide, PKKKRKV sequence),[19] and a fluorescent fluorescein tag for microscopic visualization of the probe inside cells. The fluorescein tag was needed because the croconaine chromophore was not sufficiently fluorescent for high contrast microscopy.

The lysosome targeted probe is non-fluorescent **LysoCR** (Scheme 1c) and its structure is comprised of a central croconaine with two appended morpholine groups as lysosome targeting units. The ability of morpholine units to promote probe accumulation in lysosomes is attributed to formation of protonated structures at the lysosomal acidic pH.[20] We reasoned that attaching a fluorescein might prevent lysosome accumulation; therefore, we chose to make **LysoSQ** as a highly fluorescent deep-red squaraine[21,22] analogue of **LysoCR** that does

not absorb the photothermal 808 nm laser light but permits visualization of lysosome location and structural integrity. The synthetic routes and compound characterization for all probes are provided in the ESI (Figure S1–S7) along with a summary of absorption and fluorescence properties (Figure S8–S10).

The photothermal performances of **NucCR**, **NucCR'** and **LysoCR** were assessed as a function of laser irradiation time (Figure S11) and laser power density (Figure S12). With each probe at a concentration of 20 μM and power density of 5 W/cm^2, the temperature within the spot of the laser beam increased by about 14 °C over 10 min. As shown in Figure S13, **NucCR**, **NucCR'** and **LysoCR** were subjected to four cycles of laser irradiation for 10 min followed by a cooling period without laser irradiation. Each sample showed negligible change in maximum temperature over the four iterations, reflecting very high photothermal stability. Additional cuvette studies tested probe stability under conditions that mimic the intracellular environment. These studies found no change in probe absorption or fluorescence after 30 minutes exposure to the biological thiols, glutathione (GSH), cysteine (Cys) or homocysteine (Hcy) (Figure S14–S15). Taken together, the photothermal heating and stability studies strongly indicate that **NucCR**, **NucCR'** and **LysoCR** are all excellent candidates for photothermal heating inside cells.

Cell microcopy experiments evaluated the capabilities of targeted croconaine probes **NucCR** and **NucCR'** to permeate living cells and accumulate in the nucleus. MCF-7 (human breast cancer) cells were first incubated with 10 μM **NucCR** or **NucCR'** for 2 h, and then further incubated with nuclear stain Hoechst 33342. There was excellent colocalization of **NucCR** and Hoechst 33342 fluorescence with a high Pearson's correlation coefficient (PCC) of 0.90 (Figure 1), indicating that **NucCR** accumulated predominantly in the cell nucleus. Also shown in Figure 1-d1 is a representative cross-sectional analysis of a single cell in the blue and green fluorescence channels showing close spatial overlap of the signals. The same colocalization analysis on cells treated **NucCR'** revealed a significantly lower PCC of 0.74 indicating that **NucCR'** has less specificity for the cell nucleus. The microscopy colocalization experiments were repeated with CHO-K1 cells (Chinese hamster ovary) and the same trend was observed (Figure S16); that is, the nucleus targeting capabilities of **NucCR** and **NucCR'** were high and moderate, respectively.

Standard methyl thiazolyl tetrazolium (MTT) assays revealed that MCF-7 cells treated with 20 μM **NucCR** or **NucCR'** were mostly alive (> 94%) after 2 h without light irradiation, indicating negligible dark toxicity in both cases (Figure 2a). But there was a significant difference in phototoxicity. Cells that were treated with **NucCR'** and irradiated with a laser at 808 nm (5 W/cm^2, 10 min) were 94% viable; whereas, cells that were treated with **NucCR** and laser irradiated were 58% viable. When the dose of **NucCR** or **NucCR'** was increased to 50 μM, the same laser irradiation conditions produced a further reduction in cell viability (Figure 2b). Laser induced cell death was independently confirmed by microscopic imaging using a green emitting stain for living cells (Calcein AM) and a red emitting stain for dead cells (PSVue 643).[23] As shown in Figure 3c, a typical field of **NucCR**-treated and laser-irradiated cells presented a large empty area, which indicated that the cells were dead and no longer attached to the bottom of the slide. Furthermore, the ratio of red (dead) to green (living) cells was lower for the cell population treated with **NucCR'** compared to that

of **NucCR**. Additional fluorescence microcopy studies quantified cell nucleus shrinkage (karyopyknosis) as a diagnostic indicator of cell death (Figure 2d). There was more shrinkage of cell nuclei in populations of **NucCR-**treated cells compared to **NucCR'-**treated cells. More specifically, the nuclei area of **NucCR**-treated cells decreased an average of 57%, which was more shrinkage than that observed in **NucCR'**-treated cells (decreased by 39%) (Figure S17). These independent cell death measurements consistently show that laser-induced heating of cells treated with **NucCR** causes more cell death than **NucCR'**. Even though the intracellular amounts of **NucCR** and **NucCR'** are the same and the overall amount of sample heating is the same, there is a higher fraction of **NucCR** in the cell nucleus. The implication of this finding is that the cell nucleus is sensitive to photothermal disruption and that a major outcome is cell death.

The next set of cell studies examined the properties of non-fluorescent croconaine conjugate **LysoCR** and its highly fluorescent squaraine analogue **LysoSQ**. To prove that the appended morpholine groups promote lysosome accumulation, we incubated MCF-7 cells with **LysoSQ** for 2 h, and then treated the cells with Lysotracker Yellow. As shown in Figure S18, there was strong colocalization of the deep-red fluorescence for **LysoSQ** with the green fluorescence of Lysotracker Yellow (PCC = 0.93). A subsequent series of 808 nm laser irradiation (same laser irradiation condition with **NucCR**) experiments were conducted using MCF-7 cells that were treated with different amounts of **LysoCR**. Although **LysoCR** produces the same amount of photothermal heating as **NucCR** (Figure S11), there was no measurable laser-induced phototoxicity in cells treated with up to 100 μM of **LysoCR** (Figure 3a). We conclude that laser-induced photothermal heating of the lysosomes in MCF-7 cells using **LysoCR** is substantially less phototoxic than photothermal heating the nucleus of the same cell line (using **NucCR**).

There are a few literature reports suggesting that photothermal heating of lysosomes can disrupt the surrounding membrane and promote escape of lysosomal contents.[24,25] Therefore, we explored the possibility of non-toxic near-infrared photothermal disruption of lysosomes using **LysoCR**. MCF-7 cells were co-incubated with **LysoCR** (non-fluorescent photothermal agent), deep-red fluorescent **LysoSQ**, and blue fluorescent Hoechst 33342 and the fluorescence micrographs showed the expected punctate deep-red fluorescence of **LysoSQ** within the lysosomes (Figure 3b). Subsequent 808 nm laser irradiation of these co-incubated cells induced the **LysoSQ** fluorescence to become spread diffusely throughout the cytoplasm (Figure 3b). This change in **LysoSQ** fluorescence suggested lysosomal escape of the **LysoSQ** due to photothermal heating of the lysosomes by the colocalized **LysoCR**. We hypothesized that this putative photothermal disruption of lysosomal membranes should produce changes in lysosomal pH. More specifically, the acidic pH of the lysosomes should increase if there is photothermal-induced equilibration with the near neutral pH of the cell cytosol.[26,27] This hypothesis was confirmed by conducting a set of microscopy studies that used acridine orange (AO) as a fluorescent pH sensor that emits red fluorescence when in acidic lysosomes and green fluorescence when the pH is near neutral.[28] Thus, MCF-7 cells were incubated sequentially with **LysoCR** for 2 h, followed by AO for 10 min. Before laser irradiation, many red fluorescent dots were observed, validating the presence of intact acidic lysosomes containing AO (Figure 3c). After 10 min. of near-infrared laser irradiation the red

fluorescence AO signal disappeared (Figure 3c), indicating an increase in lysosomal pH presumably due to photothermal disruption of the lysosomal membrane. The fact that the near-infrared photothermal heating does not cause cell death is consistent with literature knowledge that disrupted lysosomes are able to self-repair.[29] This finding of photothermal lysosome membrane permeabilization may have important practical applications since lysosome escape is one the major barriers preventing cytosolic delivery of chemotherapeutics, especially biological macromolecules such as proteins and antibodies.[30] In this respect, it is worth noting that lysosome escape methods that are based on oxygen photosensitization have the inherent problem that the reactive oxygen species can destroy sensitive payload. In contrast, a “clean” photothermal heating process using a croconaine probe like **LysoCR** is less likely to damage the payload.

In summary, a near-infrared croconaine-peptide conjugate that targets the cell nucleus with high specificity promoted more laser-induced cell death than an analogous probe with less nucleus specificity. The same laser irradiation conditions produced no cell phototoxicity when a croconaine-morpholine conjugate was used to target the cell lysosomes. Instead, non-toxic photothermal disruption of the lysosomes was observed which is a potentially useful way to promote intracellular delivery of imaging probes or chemotherapeutics. It should be possible to synthetically expand the portfolio of croconaine conjugates to include near-infrared photothermal probes with selective affinity for other organelles. We are grateful for funding support from the US NIH (R01GM059078 and R35GM136212) and the China Scholarship Council (CSC).

Supplementary Material

Refer to Web version on PubMed Central for supplementary material.

Notes and references

1. Qin Z and Bischof JC, Chem. Soc. Rev, 2012, 41, 1191–1217. [PubMed: 21947414]
2. Minai L, Yeheskely-Hayon D, Golan L, Bisker G, Dann EJ and Yelin D, Small, 2012, 8, 1732–1739. [PubMed: 22431265]
3. Liu Y, Bhattarai P, Dai Z and Chen X, Chem. Soc. Rev, 2019, 48, 2053–2108. [PubMed: 30259015]
4. Jung HS, Verwilst P, Sharma A, Shin J, Sessler JL and Kim JS, Chem. Soc. Rev, 2018, 47, 2280–2297. [PubMed: 29528360]
5. Gao P, Pan W, Li N and Tang B, ACS Appl. Mater. Interfaces, 2019, 11, 26529–26558. [PubMed: 31136142]
6. Wen Y, Schreiber CL and Smith BD, Bioconjug. Chem, 2020, 31, 474–482. [PubMed: 31940166]
7. Wang H, Chang J, Shi M, Pan W, Li N and Tang B, Angew. Chem. Int. Ed, 2019, 58, 1057–1061.
8. Jung HS, Lee JH, Kim K, Koo S, Verwilst P, Sessler JL, Kang C and Kim JS, J. Am. Chem. Soc, 2017, 139, 9972–9978. [PubMed: 28644025]
9. Chen D, Zhang J, Tang Y, Huang X, Shao J, Si W, Ji J, Zhang Q, Huang W and Dong X, J. Mater. Chem. B, 2018, 6, 4522–4530. [PubMed: 32254669]
10. Tan X, Luo S, Long L, Wang Y, Wang D, Fang S, Ouyang Q, Su Y, Cheng T and Shi C, Adv. Mater, 2017, 29, 1–9.
11. Spence GT, Hartland GV and Smith BD, Chem. Sci, 2013, 4, 4240–4244.
12. Guha S, Shaw SK, Spence GT, Roland FM and Smith BD, Langmuir, 2015, 31, 7826–7834. [PubMed: 26149326]

13. Yu F, Zhang F, Tang L, Ma J, Ling D, Chen X and Sun X, J. Mater. Chem. B, 2018, 6, 5362–5367. [PubMed: 30931124]
14. Chen Q, Liu X, Zeng J, Cheng Z and Liu Z, Biomaterials, 2016, 98, 23–30. [PubMed: 27177219]
15. Tang L, Yu F, Tang B, Yang Z, Fan W, Zhang M, Wang Z, Jacobson O, Zhou Z, Li L, Liu Y, Kiesewetter DO, Tang W, He L, Ma Y, Niu G, Zhang X and Chen X, ACS Appl. Mater. Interfaces, 2019, 11, 27558–27567. [PubMed: 31317730]
16. Jung HS, Han J, Lee JH, Lee JH, Choi JM, Kweon HS, Han JH, Kim JH, Byun KM, Jung JH, Kang C and Kim JS, J. Am. Chem. Soc, 2015, 137, 3017–3023. [PubMed: 25662739]
17. Pan GY, Jia HR, Zhu YX, Wang RH, Wu FG and Chen Z, ACS Biomater. Sci. Eng, 2017, 3, 3596–3606.
18. Xiang H, Xue F, Yi T, Tham HP, Liu JG and Zhao Y, ACS Appl. Mater. Interfaces, 2018, 10, 16344–16351. [PubMed: 29697957]
19. Wang HY, Chen JX, Sun YX, Deng JZ, Li C, Zhang XZ and Zhuo RX, J. Control. Release, 2011, 155, 26–33. [PubMed: 21187118]
20. Gao P, Pan W, Li N and Tang B, Chem. Sci, 2019, 10, 6035–6071. [PubMed: 31360411]
21. Anees P, Sudheesh KV, Jayamurthy P, Chandrika AR, Omkumar RV and Ajayaghosh A, Chem. Sci, 2016, 7, 6808–6814. [PubMed: 28042467]
22. Sudheesh KV, Jayaram PS, Samanta A, Bejoymohandas KS, Jayasree RS and Ajayaghosh A, Chem- A Eur. J, 2018, 24, 10999–11007.
23. Harmatys KM, Battles PM, Peck EM, Spence GT, Roland FM and Smith BD, Chem. Commun, 2017, 53, 9906–9909.
24. Chen G, Ding L, Wu P, Zhou Y, Sun M, Wang K and Oupický D, Polym. Adv. Technol, 2018, 29, 2593–2600.
25. Yang X, Fan B, Gao W, Li L, Li T, Sun J, Peng X, Li X, Wang Z, Wang B, Zhang R and Xie J, Int. J. Nanomedicine, 2018, 13, 4333–4344. [PubMed: 30087564]
26. Wen Y, Zhang W, Liu T, Huo F and Yin C, Anal. Chem, 2017, 89, 11869–11874. [PubMed: 28992693]
27. Wan Q, Chen S, Shi W, Li L and Ma H, Angew. Chem. Int. Ed, 2014, 53, 10916–10920.
28. Zhu YX, Jia HR, Pan GY, Ulrich NW, Chen Z and Wu FG, J. Am. Chem. Soc, 2018, 140, 4062–4070. [PubMed: 29406728]
29. Wang F and Boya RGP, Traffic, 2018, 19, 918–931. [PubMed: 30125440]
30. Domagala A, Fidyt K, Bobrowicz M, Stachura J, Szczygiel K and Firczuk M, Int. J. Mol. Sci, 2018, 19, 1–17.

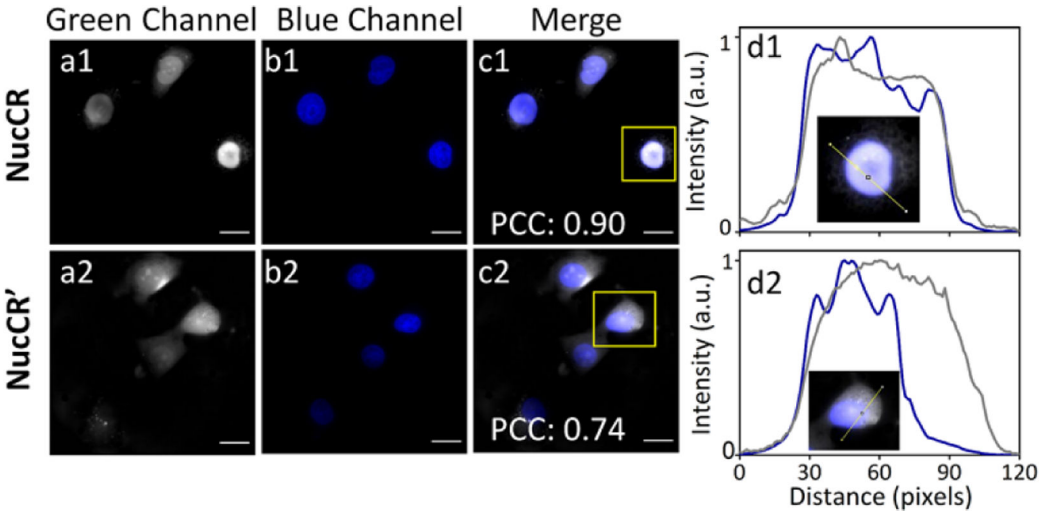

Figure 1.

Fluorescence images of live MCF-7 cells incubated with 10 μM **NucCR** (a1-c1) or **NucCR'** (a2-c2) for 2 h, and 3 μM Hoechst 33342 for an additional 15 min. Cross-sectional analysis (d1) and (d2) along the yellow line in the insets (amplified images of a single cell inside the yellow squares in c1 and c2 images, respectively). Green fluorescence channel shows location of **NucCR** or **NucCR'** (shown as grey color for clarity, ex. 450/90 nm, em. 500/50 nm); Blue channel shows location of Hoechst 33342 (ex. 387/11 nm, em. 447/60 nm). Scale bar = 20 μm.

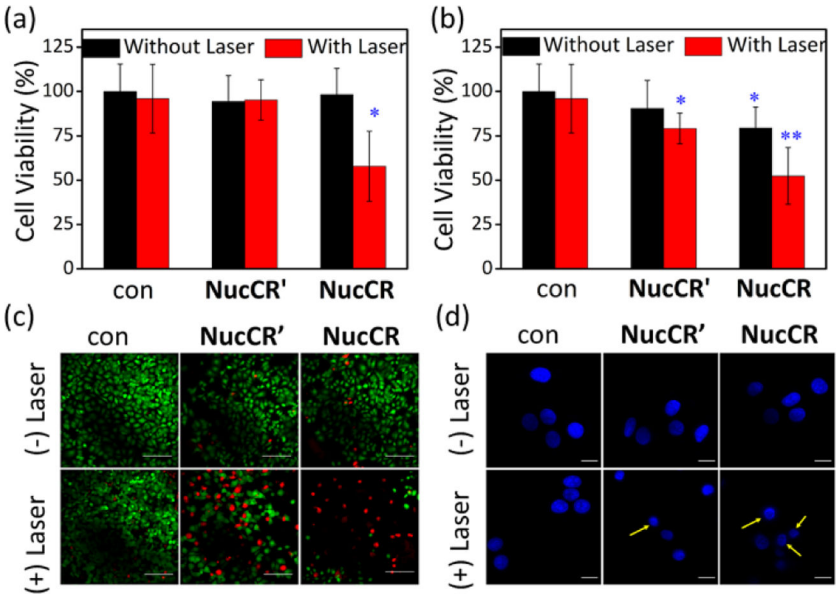

Figure 2.

Phototoxicity of **NucCR** and **NucCR'**. MCF-7 cells were first treated with (a) 20 μM or (b) 50 μM **NucCR** or **NucCR'** for 2 h, and irradiated with 808 nm laser (5 W/cm^2, 10 min), *p < 0.05, **p < 0.01. (c) Fluorescence images of MCF-7 cells treated with 20 μM **NucCR** or **NucCR'**, and laser irradiation. After irradiation, the cells were incubated for 48 h in fresh media at 37℃, and then stained with Calcein AM (1 μg/mL, indicates live cells with green fluorescence, ex. 450/90 nm, em. 500/50 nm) and PSVue643 (10 μM, indicates dead cells with deep red fluorescence, ex. 655/40 nm, em. 716/40 nm) for 30 min. Scale bar = 100 μm. (d) Micrographs of MCF-7 cell nuclei after photothermal treatment and incubation with 3 μM Hoechst 33342. Yellow arrows indicate nucleus shrinkage. Scale bar = 20 μm. Control cells (labelled as con) were not treated with **NucCR** or **NucCR'**.

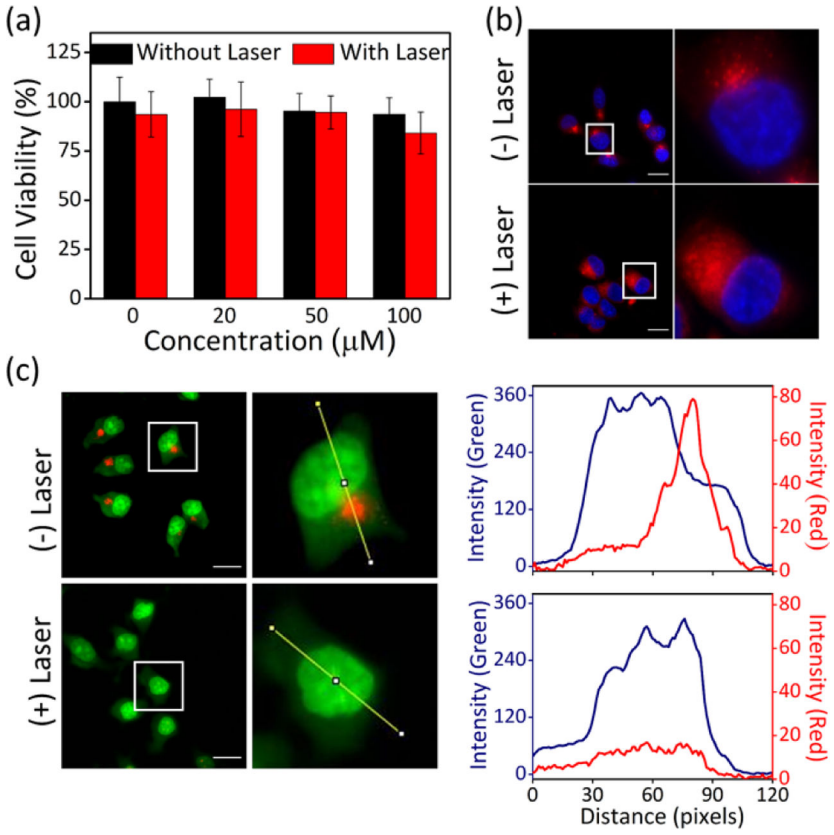

Figure 3.

(a) Viability of MCF-7 cells treated with **LysoCR** for 2 h and irradiated with 808 nm laser (5 W/cm^2, 10 min). (b) Observation of lysosomal membrane permeabilization of MCF-7 cells that had been co-incubated with 10 μM **LysoSQ** and 100 μM **LysoCR** for 2 h, irradiated with 808 nm laser (5 W/cm^2, 10 min) and then treated with Hoechst 33342. The **LysoSQ** emits deep-red fluorescence (ex. 655/40 nm, em. 716/40 nm) and the Hoechst 33342 emits blue fluorescence. (c) Effect of laser irradiation (808 nm, 5 W/cm^2, 10 min) on MCF-7 cells that had been incubated sequentially with 100 μM **LysoCR** for 2 h, followed by 1 μg/mL AO for 10 min. The AO generates red fluorescence (ex. 562/40 nm, em. 624/40 nm) in acidic lysosomes and emits green fluorescence (ex. 450/90 nm, em. 500/50 nm) at near neutral pH. Scale bar = 20 μm. Cross-sectional analysis along the yellow line in the representative cell images reflects spatial change in red (red curve) and green (blue curve) fluorescence intensity.

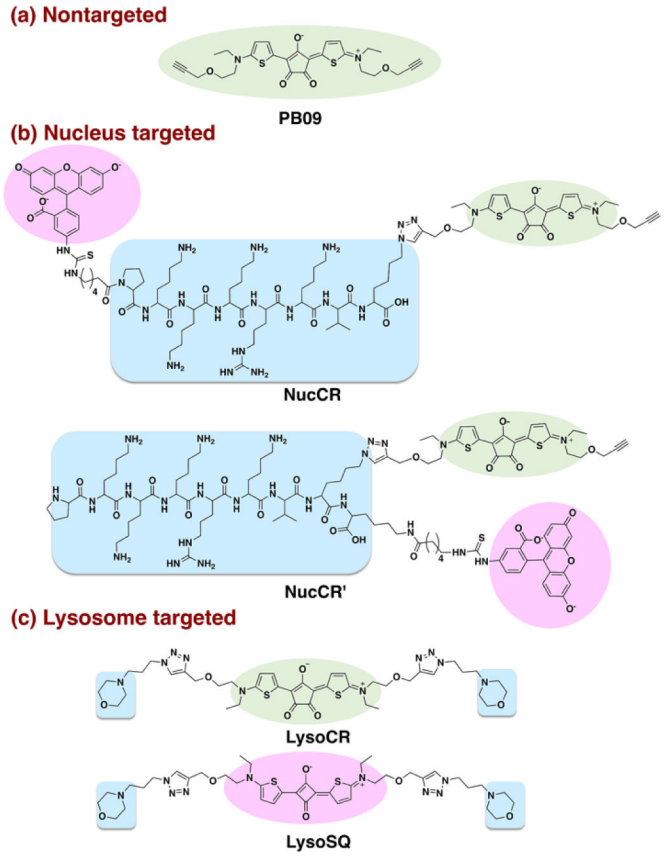

Scheme 1.

Structures of **PB09**, **NucCR**, **NucCR'**, **LysoCR** and **LysoSQ** with the following descriptors: photothermal croconaine chromophore (green), organelle targeting unit (blue), fluorescent tag (pink).